

Spin ordering-induced fully-compensated ferrimagnetism

San-Dong Guo^{1*} and Shaobo Chen² and Guangzhao Wang³

¹*School of Electronic Engineering, Xi'an University of Posts and Telecommunications, Xi'an 710121, China*

²*College of Electronic and Information Engineering,*

Anshun University, Anshun 561000, Peoples Republic of China and

³*Key Laboratory of Extraordinary Bond Engineering and Advanced Materials Technology of Chongqing, School of Electronic Information Engineering, Yangtze Normal University, Chongqing 408100, China*

Fully-compensated ferrimagnets exhibit zero net magnetic moment yet display non-relativistic global spin splitting, making them highly advantageous for constructing high-performance spintronic devices. The general strategy is to break the inversion symmetry of conventional antiferromagnets or the rotational/mirror symmetry of alternagnets to achieve fully-compensated ferrimagnets. Here, we propose to induce fully-compensated ferrimagnetism by engineering the spin ordering rather than modifying the lattice structure. Bilayer stacking engineering offers a convenient platform to verify our proposal and readily enables switching between two distinct electronic states by tuning the Néel vector of one layer. By the first-principles calculations, a bilayer system is constructed with monolayer $\text{Cr}_2\text{C}_2\text{S}_6$ as the elementary building block to corroborate our proposal. This strategy can also be extended to inducing alternagnetism via spin ordering engineering. Our work offers an alternative route to realize non-relativistic spin splitting in zero-net-magnetization magnets, paving the way for the advancement and construction of low-power spintronic device .

Introduction.— Magnetism is a cornerstone of modern technology, and among magnetic materials, ferromagnets have long commanded the spotlight, driving decades of intensive research and ubiquitous applications[1]. A paradigm shift, however, is emerging with zero-net-magnetization systems. These magnets-free from any stray fields-deliver superior spintronic performance: ultrahigh data densities, immunity to external perturbations, and femtosecond-scale writing speeds[2, 3]. Symmetry dictates that collinear, zero-net-magnetization magnets fall into three principal categories: PT -antiferromagnets (the joint symmetry (PT) of space inversion symmetry (P) and time-reversal symmetry (T)), alternagnets and fully-compensated ferrimagnets[4–7].

In PT -antiferromagnets, the PT symmetry enforces global spin degeneracy across the entire Brillouin zone (BZ), forbidding such hallmark phenomena as the magneto-optical response, anomalous Hall effect, and anomalous valley Hall effect[6, 8]. Alternagnets, by contrast, retain the real-space appearance of a collinear antiferromagnet-every spin is microscopically compensated-yet in momentum space they inherit and extend the essence of ferromagnetism. Without invoking relativistic effects, they exhibit robust spin splitting whose symmetry is classified by d -, g -, or i -wave representations[4, 5]. Consequently, alternagnets have been shown to host a suite of effects once regarded as the exclusive domain of ferromagnets: non-relativistic lifting of Kramers degeneracy, anomalous Hall and Nernst responses, spin-polarized charge currents, and the magneto-optical Kerr effect[8].

Fully-compensated ferrimagnets constitute a distinct branch of ferrimagnetism whose macroscopic moment vanishes[7, 9–11]. Across the entire BZ, they exhibit a momentum-independent, s -wave spin splitting. Like

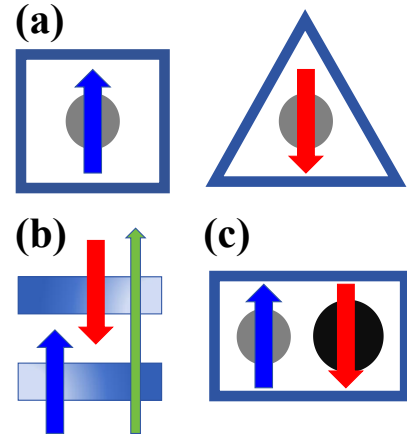


FIG. 1. (Color online)(a):the magnetic atoms with opposite spin polarization have different environment, producing fully-compensated ferrimagnetism. (b): the layer-dependent opposite spin polarization in PT -antiferromagnets and alternagnets can give rise to fully compensated ferrimagnetism under an applied electric field-whether it is an external field, the built-in field arising from a Janus structure, or the internal field of ferroelectric polarization. (c): in PT -antiferromagnets or alternagnets, the fully-compensated ferrimagnetism can be induced via isovalent alloying. In (a, b, c), the blue and red arrows represent spin-up and spin-down, respectively. In (b), the green arrow denotes the electric field. In (c), for example, the small gray sphere and the large black sphere represent $3d$ and $4d$ elements from the same chemical group, respectively.

alternagnets, fully-compensated ferrimagnets therefore give rise to phenomena: the anomalous Hall and Nernst effects, non-relativistic spin-polarized currents and the magneto-optical Kerr effect. Very recently, bilayer CrPS_4 can be electrically engineered into a fully-compensated ferrimagnet: a perpendicular gate field toggles the conduction-band spin polarization on and off, offering

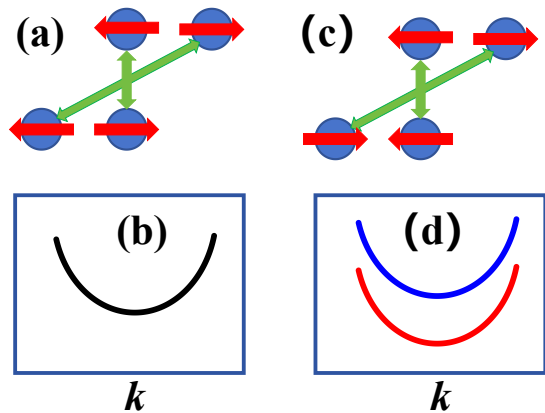


FIG. 2. (Color online) Ignoring the spin ordering, both (a) and (c) possess lattice P symmetry. When considering the spin ordering, (a) has $[C_2||P]$ symmetry, while (c) does not have $[C_2||P]$ symmetry and also lacks $[C_2||M]$ and $[C_2||C]$ symmetry. The (b) and (d) are the energy band structures corresponding to (a) and (c), respectively. In (a) and (c), the red arrows represent the spin direction, while the green arrows indicate that two atoms are connected by P symmetry. In (b) and (d), the black lines represent spin degeneracy, while the blue and red lines represent spin-up and spin-down states, respectively.

an all-electric spin switch[12]. Fully-compensated ferrimagnets can be obtained by breaking both the $[C_2||P]$ symmetry of PT -antiferromagnets and the $[C_2||C]$ or $[C_2||M]$ symmetry of altermagnets, where C_2 is the two-fold rotation perpendicular to the spin axis in spin space, and C/M means rotation/mirror symmetry in lattice space[6, 7, 13]

Previous strategies have always relied on engineering the lattice so that spin-opposite magnetic atoms reside in inequivalent environments[14]-i.e., with different surrounding atomic arrangements-to realize fully-compensated ferrimagnets (See Figure 1 (a)). For example, the layer-dependent opposite spin polarization exists in PT -antiferromagnets and altermagnets, which can transform into fully-compensated ferrimagnets under an applied electric field-whether it is an external field, the built-in field arising from a Janus structure, or the internal field of ferroelectric polarization (See Figure 1 (b)) [6, 7, 13]. For instance, fully-compensated ferrimagnetism can also be achieved via isoelectronic alloying (See Figure 1 (c))[6, 7, 9–11, 13]. Indeed, in both PT -antiferromagnets and altermagnets, fully-compensated ferrimagnetism can also be realized by perturbing the environment around one spin-polarized atom through doping or vacancies[14, 15]. A natural question is whether alternative strategies exist to realize fully-compensated ferrimagnetism. Here, we propose an alternative route to fully-compensated ferrimagnetism: instead of tailoring the lattice, we engineer the spin ordering.

Approach.— To achieve spin ordering-induced fully-compensated ferrimagnetism, the primitive unit cell

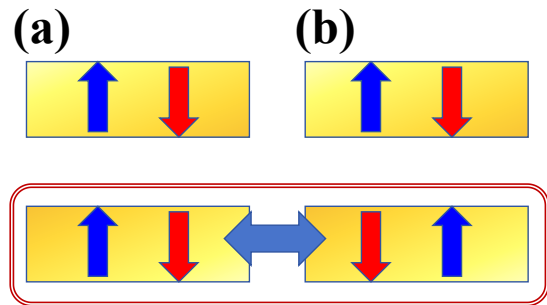


FIG. 3. (Color online) By bilayer stacking engineering, (a) has $[C_2||P]$ symmetry, while (b) does not have $[C_2||P]$ symmetry and also lacks $[C_2||M]$ and $[C_2||C]$ symmetry. The transition between (a) and (b) can be realized by controlling the Néel vector of the lower layer to flip by 180° . The blue and red arrows represent spin-up and spin-down, respectively.

should generally contain at least four magnetic atoms, as shown in Figure 2 (a) and (c). When ignoring the spin ordering, both Figure 2 (a) and (c) possess lattice P symmetry. When considering the spin ordering, Figure 2 (a) has $[C_2||P]$ symmetry, which leads to spin degenerate due to $[C_2||P][C_2||T]$ symmetry ($E_\uparrow(k)=[C_2||P][C_2||T]E_\uparrow(k)=[C_2||P]E_\uparrow(-k)=E_\downarrow(k)$), as shown in Figure 2 (b). In fact, Figure 2 (a) shows PT -antiferromagnetism. When considering the spin ordering, Figure 2 (c) does not possess $[C_2||P]$ symmetry. This broken $[C_2||P]$ symmetry will induce spin splitting. However, if $[C_2||M/C]$ symmetry is present, it will lead to altermagnetism ($E_\uparrow(k)=[C_2||M/C]E_\uparrow(k)=E_\downarrow(M/Ck)$)[4, 5]. If these two symmetries are also excluded, it will result in fully-compensated ferrimagnetism with global spin splitting (see Figure 2 (d))[7]. From Figure 2 (a) to (c), simply changing the spin ordering without altering the atomic arrangement can induce fully-compensated ferrimagnetism, achieving global spin splitting.

It may be difficult to directly find the material we propose. Here, we achieve our proposal through bilayer stacking engineering, which has already served as a versatile platform for realizing diverse electronic states[16–19]. For example, we first search for monolayer that contain two magnetic atoms with antiferromagnetic (AFM) coupling, which is used as the basic building unit. Subsequently, by employing operations such as reflection, rotation, and translation on the basic building unit, we construct a bilayer that fulfills the lattice P symmetry. The spin-degenerate and globally spin-splitting states, that is, PT -antiferromagnetism and fully-compensated ferrimagnetism, can be interconverted by manipulating the Néel vector of the lower layer, specifically by flipping the Néel vector by 180° (see Figure 3). Experimentally, the switching of Néel vector can be realized by spin-orbit torques, and the reorientation of Néel vectors with 180° switching has been realized experimentally[20].

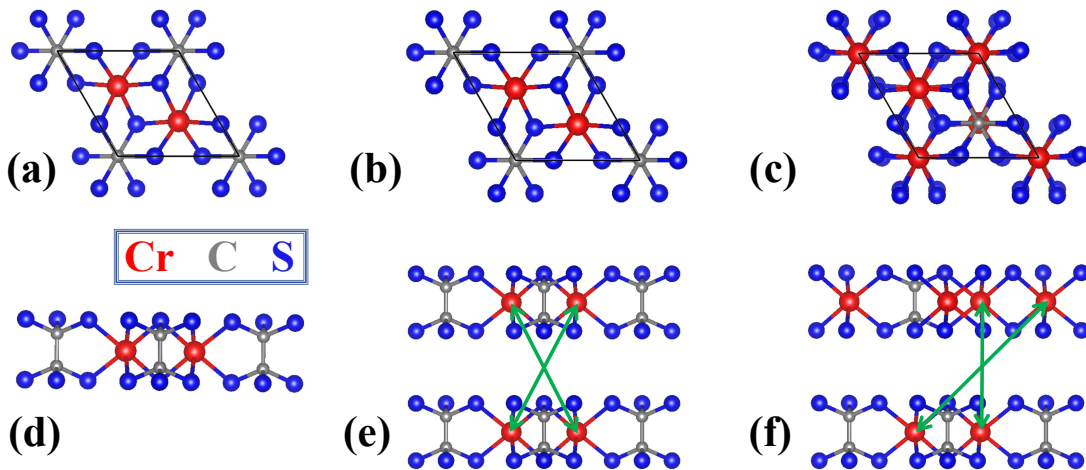


FIG. 4. (Color online) The top (a, b, c) and side (d, e, f) views of the crystal structures of monolayer $\text{Cr}_2\text{C}_2\text{S}_6$ (a, d), bilayer A-stacked $\text{Cr}_2\text{C}_2\text{S}_6$ (b, e) and bilayer B-stacked $\text{Cr}_2\text{C}_2\text{S}_6$ (c, f). In (e) and (f), the green arrows indicate that two Cr atoms are connected by P symmetry.

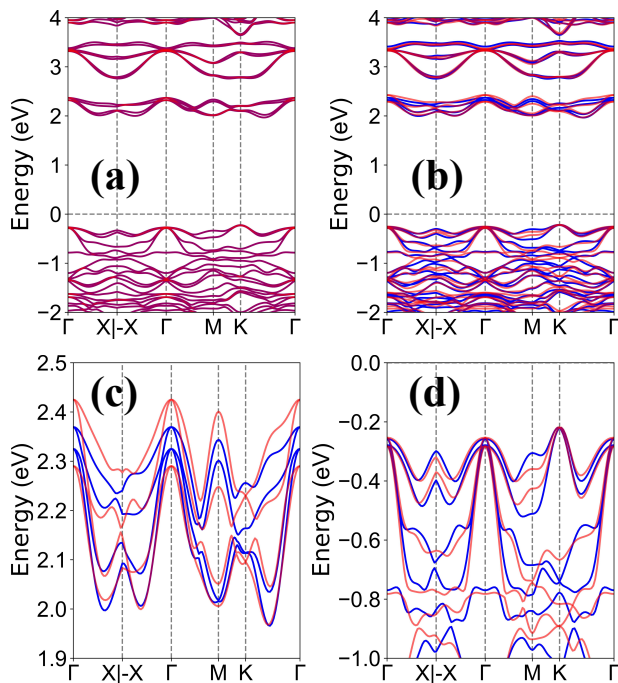


FIG. 5. (Color online) The energy band structures of bilayer B-stacked $\text{Cr}_2\text{C}_2\text{S}_6$ with PT symmetry (a) and without PT symmetry (b). The (c) and (d) are the enlargements of the conduction and valence bands near the Fermi level for (b). The spin-up and spin-down channels are depicted in blue and red, and the purple color means spin degeneracy.

Computational detail.— The spin-polarized first-principles calculations are performed within density functional theory (DFT)[21] using the Vienna Ab Initio Simulation Package (VASP)[22–24]. We employ the Perdew-Burke-Ernzerhof generalized gradient approximation (PBE-GGA)[25] as the exchange-correlation functional. The calculations are carried out with the ki-

netic energy cutoff of 500 eV, total energy convergence criterion of 10^{-8} eV, and force convergence criterion of $0.001 \text{ eV} \cdot \text{\AA}^{-1}$. To account for the localized nature of Cr-3d orbitals, we use a Hubbard correction U_{eff} within the rotationally invariant approach proposed by Dudarev et al[26]. The $U_{eff}=3.0$ eV[13, 27] and 3.55 eV[28, 29] are used for $\text{Cr}_2\text{C}_2\text{S}_6$ and Cr_2SO , respectively. A vacuum layer exceeding 16 Å along the z -direction is employed to eliminate spurious interactions between periodic images. The BZ is sampled with a $15 \times 15 \times 1$ Monkhorst-Pack k -point mesh for both structural relaxation and electronic structure calculations.

Material realization.— Here, the monolayer $\text{Cr}_2\text{C}_2\text{S}_6$ is used as the basic building unit, which has been proved to be dynamically, mechanically and thermally stable[13]. As shown in Figure 4 (a) and (d), there are two Cr atoms in the primitive unit cell, which are surrounded by six S atoms, and the two CrS_3 moieties are connected by two C atoms. The $\text{Cr}_2\text{C}_2\text{S}_6$ crystallizes in the $P\bar{3}1m$ space group (No.162) with P and M symmetries, which transform one Cr sublattice into the other. The magnetic ground state of $\text{Cr}_2\text{C}_2\text{S}_6$ among ferromagnetic (FM), AFM-Néel (AFM1), AFM-stripy (AFM2) and AFM-zigzag (AFM3) magnetic configurations is AFM1 ordering (See FIG.S1[30]), and the energy differences between FM/AFM2/AFM3 and AFM1 orderings are 266 meV, 167 meV and 114 meV, respectively. Within AFM1 ordering, the optimized lattice constants are $a=b=5.636$ Å for monolayer $\text{Cr}_2\text{C}_2\text{S}_6$.

Then, we construct the bilayer structure, with $\text{Cr}_2\text{C}_2\text{S}_6$ as the lower layer, and the upper layer can be obtained through a horizontal mirror operation, which is named as bilayer A-stacked $\text{Cr}_2\text{C}_2\text{S}_6$, as shown in Figure 4 (b) and (e). The bilayer A-stacking also crystallizes in the $P\bar{3}1m$ space group (No.162), possessing lattice P symmetry. However, after the $[C_2||P]$ is broken by tuning the

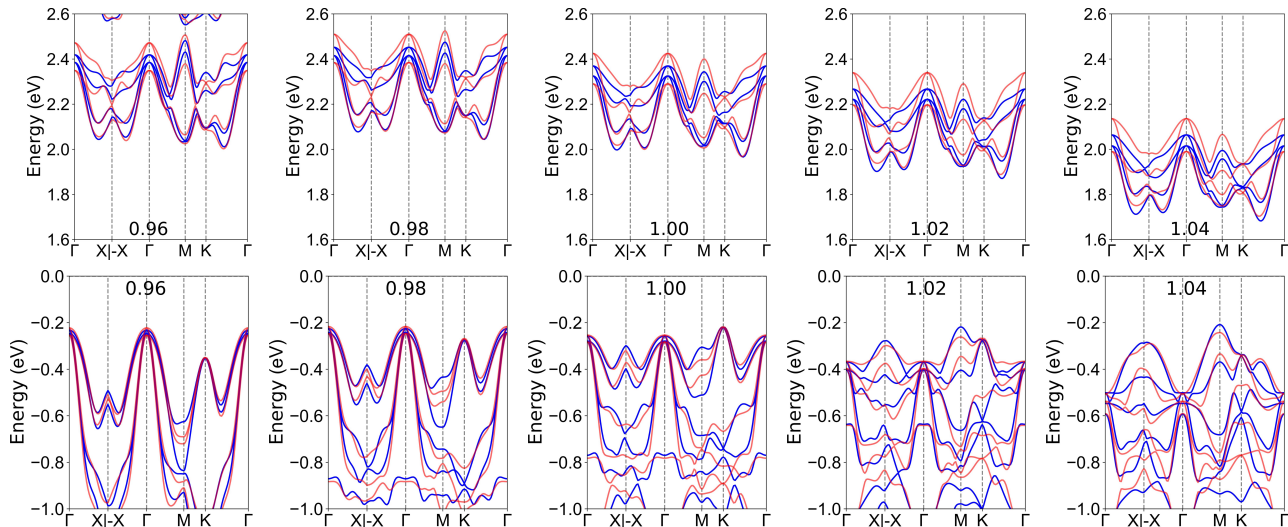


FIG. 6. (Color online) The enlargements of the conduction (top) and valence (bottom) bands near the Fermi level for bilayer B-stacked $\text{Cr}_2\text{C}_2\text{S}_6$ without PT symmetry at representative a/a_0 (0.96, 0.98, 1.00, 1.02 and 1.04). The spin-up and spin-down channels are depicted in blue and red.

spin ordering, it still possesses $[C_2\|M]$, which will result in altermagnetism, a subject to be discussed later. In addition, the energy of this type of bilayer stacking is generally not a minimum. By translating the top sublayer by $(\vec{a}/3+2\vec{b}/3)$, the bilayer B-stacked $\text{Cr}_2\text{C}_2\text{S}_6$ can be obtained, as shown in Figure 4 (c) and (f). The B-stacking indeed has an energy 22 meV lower than the A-stacking. Moreover, the B-stacking still preserves the lattice P symmetry with $P\bar{3}$ space group (No.147).

Because the AFM1 ordering of monolayer $\text{Cr}_2\text{C}_2\text{S}_6$ is at least 114 meV lower in energy than any other magnetic configuration, and the interlayer coupling is extremely weak, we keep each layer $\text{Cr}_2\text{C}_2\text{S}_6$ locked in the AFM1 ordering and only vary the interlayer magnetic arrangements. For B-stacking, the magnetic ordering with PT symmetry is 1.04 meV lower in energy than that without PT symmetry. Nevertheless, given the tiny energy difference between them, the two magnetic states can be interconverted simply by tuning the Néel vector of the lower layer $\text{Cr}_2\text{C}_2\text{S}_6$. For B-stacking, once the spin order breaks $[C_2\|P]$ symmetry, neither $[C_2\|M]$ nor $[C_2\|C]$ symmetries survive, so the bilayer B-stacked $\text{Cr}_2\text{C}_2\text{S}_6$ becomes a fully-compensated ferrimagnet.

Next, we corroborate our analysis by examining the energy band structures. Since monolayer $\text{Cr}_2\text{C}_2\text{S}_6$ exhibits altermagnetism with i -wave spin-splitting symmetry under an out-of-plane electric field[13], we have added the Γ -X|X'- Γ path[31] for the related energy band structures, which is shown in FIG.S2[30]. The energy band structures of bilayer B-stacked $\text{Cr}_2\text{C}_2\text{S}_6$ with PT symmetry and without PT symmetry, along with the enlargements of the conduction and valence bands near the Fermi level for the non- PT -symmetric case, are plotted in Figure 5.

For the PT -symmetric case, the band structures

clearly exhibit spin degeneracy. For the non- PT -symmetric case, the bands show obvious spin splitting, and the band structures exhibit no symmetric connectivity along the high-symmetry paths Γ -X and X'- Γ , which is different from the case of altermagnetism. Together with the fact that the total magnetic moment of the bilayer $\text{Cr}_2\text{C}_2\text{S}_6$ is $0 \mu_B$, this confirms that bilayer B-stacked $\text{Cr}_2\text{C}_2\text{S}_6$ is indeed a fully-compensated ferrimagnet. When fully-compensated ferrimagnetism is realized via an electric field, Janus engineering or alloying, the absolute values of the magnetic moments on the magnetic atoms are unequal[6, 7]. Nevertheless, the spin ordering-induced fully-compensated ferrimagnetism yields identical absolute values of magnetic moments ($3.006 \mu_B$) on all Cr atoms in bilayer $\text{Cr}_2\text{C}_2\text{S}_6$.

Strain can effectively tune the electronic structure and magnetic properties of two-dimensional (2D) materials. Here, the ratio a/a_0 (The a and a_0 represent the strained and unstrained lattice constants, respectively) is employed to simulate biaxial strain, where $a/a_0 < 1$ ($a/a_0 > 1$) corresponds to compressive (tensile) strain. Within considered strain range ($a/a_0 = 0.96 \sim 1.04$), the magnetic ordering with PT symmetry is always lower in energy than that without PT symmetry (See FIG.S3[30]). The enlargements of the conduction and valence bands near the Fermi level for bilayer B-stacked $\text{Cr}_2\text{C}_2\text{S}_6$ without PT symmetry at representative a/a_0 are shown in Figure 6. A pivotal strain-induced effect is the controllable relocation of the valence band maximum (VBM): compressive strain drives the VBM to the Γ point, whereas tensile strain shifts it to the M point. The pronounced spin splitting at the M point of the valence band makes tensile strain more favorable for spintronic applications (See the band structure at 1.02 strain).

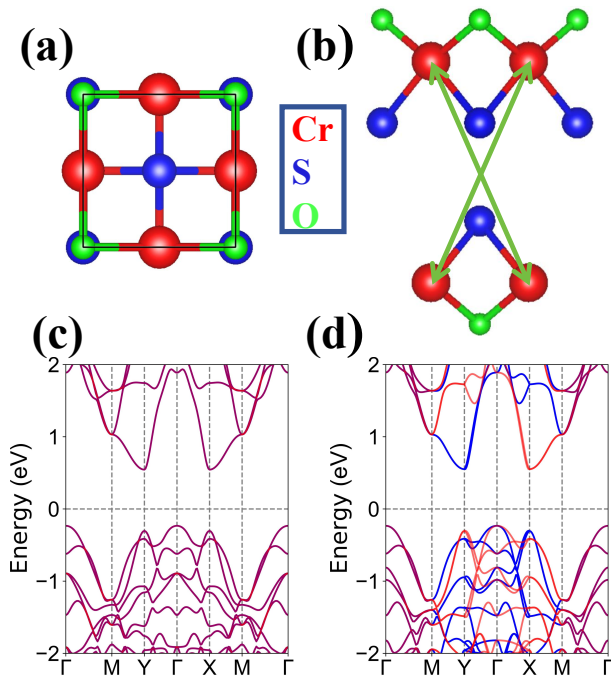


FIG. 7. (Color online) The top (a) and side (b) views of the crystal structures of bilayer B-stacked Cr_2SO . In (b), the green arrows indicate that two Cr atoms are connected by P symmetry. The energy band structures of bilayer B-stacked Cr_2SO with PT symmetry (c) and without PT symmetry but $[C_2||M]$ symmetry (d). In (c) and (d), the spin-up and spin-down channels are depicted in blue and red, and the purple color means spin degeneracy.

Discussion and conclusion.— In addition to spin ordering giving rise to fully-compensated ferrimagnetism, it can also induce altermagnetism. When Figure 2 (c) does not possess $[C_2||P]$ symmetry, but $[C_2||M]$ or $[C_2||C]$ symmetry is present, it will lead to altermagnetism. Likewise, we employ bilayer stacking engineering to corroborate our proposal. Using monolayer Cr_2SO [29] as the basic building unit, we construct S-terminal bilayer and O-terminal bilayer with lattice P symmetry as A stacking via mirror symmetry operation, which crystallizes in the $P4/mmm$ space group (No.123). The energy of O-terminal bilayer is 15 meV lower than that of S-terminal bilayer. We will focus on O-terminal bilayer, and the crystal structures of O-terminal bilayer with A stacking along with monolayer Cr_2SO are plotted in FIG.S4[30].

To obtain lower-energy stacking configuration, based on A stacking, the B stacking (See Figure 7 (a) and (b)) is obtained by translating the top sublayer by $(\vec{a}+\vec{b})/2$ along the diagonal direction. The B stacking crystallizes in $P4/nmm$ (No.129), and it has also lattice P symmetry. It is found that the energy of B stacking is approximately 114 meV lower than that of A stacking. For B-stacking, the magnetic ordering with PT symmetry is 1.13 meV higher in energy than that without PT symmetry. It is noteworthy that a magnetic ordering without PT sym-

metry can host altermagnetism when $[C_2||P]$ symmetry is absent but $[C_2||M]$ symmetry is preserved. The energy band structures of bilayer B-stacked Cr_2SO with PT symmetry and without PT symmetry are plotted in Figure 7 (c) and (d). It is evident that tuning the spin ordering enables a transition between PT -antiferromagnetism and altermagnetism. Experimentally, the transition between the two magnetic states can also be achieved by flipping the Néel vector of the lower layer Cr_2SO . In fact, bilayer A-stacked $\text{Cr}_2\text{C}_2\text{S}_6$ can likewise undergo a transition between PT -antiferromagnetism and altermagnetism via spin ordering tuning (See FIG.S5[30]), yet its energy does not correspond to a minimum. Similarly, spin symmetry-induced altermagnetism has also been achieved in $\text{Mn}_2\text{P}_2\text{Te}_6$ bilayer[32].

In summary, we present an alternative strategy for inducing fully-compensated ferrimagnetism by modulating spin ordering, which is further validated by first-principles calculations in bilayer $\text{Cr}_2\text{C}_2\text{S}_6$. The two magnetic states with and without PT symmetry can be interconverted simply by tuning the Néel vector of the lower or upper layer $\text{Cr}_2\text{C}_2\text{S}_6$. Spin ordering-driven fully-compensated ferrimagnetism equalizes the absolute magnetic moments on every Cr atom in bilayer $\text{Cr}_2\text{C}_2\text{S}_6$. This differs fundamentally from the conventional structure-modulation route, where the absolute magnetic moments of the magnetic atoms in a fully-compensated ferrimagnet are unequal. These findings establish a clear path toward exploring fully-compensated ferrimagnetism by tuning spin ordering.

This work is supported by Natural Science Basis Research Plan in Shaanxi Province of China (2025JC-YBMS-008). We are grateful to Shanxi Supercomputing Center of China, and the calculations were performed on TianHe-2.

* sandongyuwang@163.com

- [1] S. A. Wolf, D. D. Awschalom, R. A. Buhrman, J. M. Daughton, S. von Molnár, M. L. Roukes, A. Y. Chtchelkanova and D. M. Treger, Spintronics: a spin-based electronics vision for the future, *Science* **294**, 1488 (2001).
- [2] X. Hu, Half-metallic antiferromagnet as a prospective material for spintronics, *Adv. Mater.* **24**, 294 (2012).
- [3] T. Jungwirth, J. Sinova, A. Manchon, X. Marti, J. Wunderlich and C. Felser, The multiple directions of antiferromagnetic spintronics, *Nat. Phys.* **14**, 200 (2018).
- [4] L. Šmejkal, J. Sinova and T. Jungwirth, Beyond conventional ferromagnetism and antiferromagnetism: A phase with nonrelativistic spin and crystal rotation symmetry, *Phys. Rev. X* **12**, 031042 (2022).
- [5] I. Mazin, Altermagnetism—a new punch line of fundamental magnetism, *Phys. Rev. X* **12**, 040002 (2022).
- [6] S. D. Guo, Valley polarization in two-dimensional zero-net-magnetization magnets, *Appl. Phys. Lett.* **126**,

- 080502 (2025).
- [7] Y. Liu, S. D. Guo, Y. Li and C. C. Liu, Two-dimensional fully-compensated Ferrimagnetism, *Phys. Rev. Lett.* **134**, 116703 (2025).
- [8] L. Bai, W. Feng, S. Liu, L. Šmejkal, Y. Mokrousov, and Y. Yao, Altermagnetism: Exploring New Frontiers in Magnetism and Spintronics, *Adv. Funct. Mater.* **34**, 2409327 (2024).
- [9] H. van Leuken and R. A. de Groot, Half-Metallic Antiferromagnets, *Phys. Rev. Lett.* **74**, 1171 (1995).
- [10] H. Akai and M. Ogura, Half-Metallic Diluted Antiferromagnetic Semiconductors, *Phys. Rev. Lett.* **97**, 026401 (2006).
- [11] S. Wurmehl, H. C. Kandpal, G. H. Fecher, and C. Felser, Valence electron rules for prediction of half-metallic compensated-ferrimagnetic behaviour of Heusler compounds with complete spin polarization, *J. Phys.: Condens. Matter* **18**, 6171 (2006).
- [12] F. Yao, M. Liao, M. Gibertini et al., Switching on and off the spin polarization of the conduction band in antiferromagnetic bilayer transistors. *Nat. Nanotechnol.* **20**, 609 (2025).
- [13] S. D. Guo, X. S. Guo, D. C. Liang and G. Wang, Symmetry-breaking induced transition among net-zero-magnetization magnets, *J. Mater. Chem. C* **13**, 11997 (2025).
- [14] S. D. Guo, Y. L. Tao, G. Wang and Y. S. Ang, How to produce spin-splitting in antiferromagnetic materials, *J. Phys.: Condens. Matter* **36**, 215804 (2024).
- [15] L. Zhang, S. D. Guo and G. Zhu, Electric-field-induced fully-compensated ferrimagnetism in experimentally synthesized monolayer MnSe, arXiv:2503.14834 (2025).
- [16] Y. Liu, J. Yu and C. C. Liu, Twisted Magnetic Van der Waals Bilayers: An Ideal Platform for Altermagnetism, *Phys. Rev. Lett.* **133**, 206702 (2024).
- [17] J. Ji, G. Yu, C. Xu and H.J. Xiang, General Theory for Bilayer Stacking Ferroelectricity, *Phys. Rev. Lett.* **130**, 146801 (2023).
- [18] P. Jiang, C. Wang, D. Chen, Z. Zhong, Z. Yuan, Z. Y. Lu and W. Ji, Stacking tunable interlayer magnetism in bilayer CrI₃, *Phys. Rev. B* **99**, 144401 (2019).
- [19] S. D. Guo, P. Li and G. Wang, First-principles calculations study of valley polarization in antiferromagnetic bilayer systems, *Phys. Rev. B* **111**, L140404 (2025).
- [20] L. Han, X. Fu, R. Peng et al., Electrical 180° switching of Néel vector in spin-splitting antiferromagnet, *Sci. Adv.* **10**, eadn0479 (2024).
- [21] P. Hohenberg and W. Kohn, Inhomogeneous Electron Gas, *Phys. Rev.* **136**, B864 (1964); W. Kohn and L. J. Sham, Self-Consistent Equations Including Exchange and Correlation Effects, *Phys. Rev.* **140**, A1133 (1965).
- [22] G. Kresse, Ab initio molecular dynamics for liquid metals, *J. Non-Cryst. Solids* **193**, 222 (1995).
- [23] G. Kresse and J. Furthmüller, Efficiency of ab-initio total energy calculations for metals and semiconductors using a plane-wave basis set, *Comput. Mater. Sci.* **6**, 15 (1996).
- [24] G. Kresse and D. Joubert, From ultrasoft pseudopotentials to the projector augmented-wave method, *Phys. Rev. B* **59**, 1758 (1999).
- [25] J. P. Perdew, K. Burke and M. Ernzerhof, Generalized gradient approximation made simple, *Phys. Rev. Lett.* **77**, 3865 (1996).
- [26] S. L. Dudarev, G. A. Botton, S. Y. Savrasov, C. J. Humphreys, and A. P. Sutton, Electron-energy-loss spectra and the structural stability of nickel oxide: An LSDA+U study, *Phys. Rev. B* **57**, 1505 (1998).
- [27] P. Wang, D. X. Wu, K. Zhang and X. J. Wu, Two-Dimensional Quaternary Transition Metal Sulfide CrMoA₂S₆ (A = C, Si, or Ge): A Bipolar Antiferromagnetic Semiconductor with a High Néel Temperature, *J. Phys. Chem. Lett.* **13**, 3850 (2022).
- [28] X. Chen, D. Wang, L. Y. Li and B. Sanyal, Giant spin-splitting and tunable spin-momentum locked transport in room temperature collinear antiferromagnetic semimetallic CrO monolayer, *Appl. Phys. Lett.* **123**, 022402 (2023).
- [29] S.-D. Guo, X.-S. Guo, K. Cheng, K. Wang, and Y. S. Ang, Piezoelectric altermagnetism and spin-valley polarization in Janus monolayer Cr₂SO, *Appl. Phys. Lett.* **123**, 082401 (2023).
- [30] See Supplemental Material at [] for magnetic configurations, BZ with high symmetry points, energy difference as a function of a/a_0 , the related crystal structures of Cr₂SO and energy band structures of bilayer A-stacked Cr₂C₂S₆.
- [31] I. Mazin, R. González-Hernández and L. Šmejkal, Induced Monolayer Altermagnetism in MnP(S,Se)₃ and FeSe, arXiv:2309.02355 (2023).
- [32] W. Sun, W. Wang, C. Yang, S. Huang, N. Ding, S. Dong and Z. Cheng, Designing Spin Symmetry for Altermagnetism with Strong Magnetoelectric Coupling. *Adv. Sci.* **e03235** (2025).